Spinor Bose-Einstein condensate flow past an obstacle

A. S. Rodrigues,[1] P. G. Kevrekidis,[2] R. Carretero-González,[3] D. J. Frantzeskakis,[4] P. Schmelcher,[5,6] T. J. Alexander,[7] and Yu. S. Kivshar[7]

[1]*Departamento de Física/CFP, Faculdade de Ciências, Universidade do Porto, R. Campo Alegre, 687-4169-007 Porto, Portugal*
[2]*Department of Mathematics and Statistics, University of Massachusetts, Amherst, Massachusetts 01003-4515, USA*
[3]*Department of Mathematics and Statistics, Nonlinear Dynamical Systems Group,* * *and Computational Science Research Center, San Diego State University, San Diego, California 92182-7720, USA*
[4]*Department of Physics, University of Athens, Panepistimiopolis, Zografos, Athens 157 84, Greece*
[5]*Theoretische Chemie, Physikalisch-Chemisches Institut, Im Neuenheimer Feld 229, Universität Heidelberg, 69120 Heidelberg, Germany*
[6]*Physikalisches Institut, Universität Heidelberg, Philosophenweg 12, 69120 Heidelberg, Germany*
[7]*Nonlinear Physics Center, Research School of Physical Sciences and Engineering, Australian National University, Canberra ACT 0200, Australia*

(Received 7 November 2008; published 3 April 2009)

We study the flow of a spinor ($F=1$) Bose-Einstein condensate in the presence of an obstacle. We consider the cases of ferromagnetic and polar spin-dependent interactions, and find that the system demonstrates two speeds of sound that are identified analytically. Numerical simulations reveal the nucleation of macroscopic nonlinear structures, such as dark solitons and vortex-antivortex pairs, as well as vortex rings in one- and higher-dimensional settings, respectively, when a localized defect (e.g., a blue-detuned laser beam) is dragged through the spinor condensate at a speed larger than the second critical speed.

DOI: 10.1103/PhysRevA.79.043603 PACS number(s): 03.75.Mn, 03.75.Lm, 03.75.Kk

I. INTRODUCTION

Over the last decade, we have seen an enormous growth of interest and a related diversification of the physics of atomic Bose-Einstein condensates (BECs) [1,2]. A significant aspect of this ever-expanding interest is the intense study of macroscopic nonlinear excitations, such as solitons and vortices, which can arise in BECs [3]. In fact, the emergence of such macroscopic coherent structures in the many-body state of the system establishes a close connection between BECs and other branches of physics, such as, e.g., optics and the physics of nonlinear waves. Within this interface of atomic and nonlinear wave physics, in recent years there has been an increasing focus on the study of multicomponent BECs [3], and particularly *spinor condensates* [4,5]. The latter have been realized with the help of far-off-resonant optical techniques for trapping ultracold atomic gases [6] which, in turn, allowed the spin degree of freedom to be explored (previously frozen in magnetic traps). This relatively recent development has given rise to a wealth of multicomponent phenomena, including the formation of spin domains [7] and spin textures [8], spin-mixing dynamics [9], dynamic fragmentation [10], and the dynamics of quantum phases [11]. At the same time, macroscopic nonlinear structures that may arise in spinor BECs have also been investigated. Such structures include bright [12–14], dark [15], and gap solitons [16], as well as more elaborate complexes, such as bright-dark solitons [17] and domain walls [18].

A relevant direction that has been of particular interest concerns the study of the breakdown of superfluidity and the concomitant generation of excitations in BECs. In particular, much experimental and theoretical effort has been devoted to the understanding of important relevant concepts, such as the critical velocity introduced by Landau, sound waves and the speed of sound, and the emergence of vortices and solitons [1,2]. From the theoretical point of view, the Gross-Pitaevskii (GP) equation has been used to study the flow of a BEC around an obstacle or, equivalently, the effect of dragging a localized potential (such as a blue-detuned laser beam) through a BEC. In this context, it has been predicted theoretically [19–22] and recently observed experimentally [23] that when the speed of the "localized defect" exceeds a critical speed, then excitations arise, which, in the presence of (repulsive) nonlinearity, shape into dark solitons in quasi-one-dimensional (1D) condensates. On the other hand, in higher-dimensional [e.g., quasi-two-dimensional (2D)] settings, theoretical studies [24] have shown that a similar procedure leads to the formation of vortices (or more precisely to vortex-antivortex pairs due to the conservation of total topological charge). Importantly, experimental consequences of this procedure, such as an onset of heating and dissipation, were monitored experimentally [25]. Other relevant theoretical works include studies of the breakdown of superfluidity, the onset of dissipation, and the associated Landau criterion [26]. The Landau criterion for the breakdown of superfluidity is intimately connected to the emergence of excitations (be they linear phononlike for weak defects, or solitonic for stronger defects or more significant nonlinearity). This is because the emission of such excitations renders the flow nonstationary, which in turn, as explained in Ref. [24] (see also Ref. [26]), produces a nonvanishing drag force associated with the presence of dissipation. More recently, dragging of an obstacle in a two-component BEC was studied in Ref. [27]. In this latter study it was established that two distinct "speeds of sound" arise and the form of the ensuing nonlinear structures (e.g., dark-dark or dark-antidark soliton pairs

*http://nlds.sdsu.edu

in 1D, and vortex-vortex or vortex-lump pairs in 2D) depend on how the value of the obstacle speed compares to the values of the critical speeds.

In this paper, we consider the dragging of a localized defect through an $F=1$ spinor condensate with repulsive spin-independent interactions and either ferromagnetic or antiferromagnetic (polar) spin-dependent interactions. In the framework of mean-field theory, this system is described by a set of coupled GP equations for the wave functions of the three hyperfine components. A key question that emerges in this $F=1$ spinor BEC setting is how many critical speeds may be available. A naive count based on the three-component nature of the system (and by analogy to the two-component setting bearing two such critical speeds) would suggest the possibility for three distinct critical speeds. However, as we illustrate below, an explicit calculation reveals that there exist only two such critical speeds in the system due to the particular nature of the nonlinearity. Moreover, our numerical simulations illustrate that the crossing of the lower of the two critical speeds does not appear to lead to the formation of nonlinear excitations. On the other hand, for defect speeds larger than the second critical speed, our simulations illustrate that dark solitons emerge in the 1D setting, vortex-antivortex pairs in the 2D setting, and vortex rings are shown to arise in the fully three-dimensional (3D) setting.

The presentation of our results is structured as follows. In Sec. II, we develop an analytical approach for computing the relevant critical speeds by generalizing to the spinor setting the arguments of Ref. [19]. Then, in Sec. III, we numerically test the relevant predictions in 1D, 2D, and 3D settings. Finally, in Sec. IV, we summarize our findings and point to some important remaining questions along this vein of research.

II. MODEL AND ITS ANALYSIS

In our analytical approach, we will consider a quasi-1D spinor $F=1$ BEC with repulsive spin-independent interactions. In the framework of mean-field theory, this system can be described by the following normalized GP equations [17,18]:

$$i\partial_t\psi_{\pm 1} = H_0\psi_{\pm 1} + r[(|\psi_{\pm 1}|^2 + |\psi_0|^2 - |\psi_{\mp 1}|^2)\psi_{\pm 1}] + r\psi_0^2\psi_{\mp 1}^*, \tag{1}$$

$$i\partial_t\psi_0 = H_0\psi_0 + r[(|\psi_{-1}|^2 + |\psi_{+1}|^2)\psi_0] + 2r\psi_{-1}\psi_0^*\psi_{+1}, \tag{2}$$

where $H_0 \equiv -(1/2)\partial_x^2 + V(x;t) + n_{\mathrm{tot}}$ while $n_{\mathrm{tot}} = |\psi_{-1}|^2 + |\psi_0|^2 + |\psi_{+1}|^2$ is the total density and $V(x;t)$ is the external potential. The latter is assumed to take the following form:

$$V(x;t) = \frac{1}{2}\Omega^2 x^2 + V_0 \exp[-a(x-st)^2]. \tag{3}$$

The first term in the right-hand side of Eq. (3) represents a typical harmonic trapping potential of normalized strength Ω while the second term accounts for a localized repulsive potential (e.g., a blue-detuned laser beam) of strength V_0 and width a^{-1}, which is dragged through the condensate at speed s. Note that our analytical results will be obtained below for the case of $\Omega=0$ (which still contains the fundamental phenomenology) but were also tested in the numerical simulations for $\Omega \neq 0$ (and were found to persist in the latter case). Finally, the parameter r in Eqs. (1) and (2) expresses the normalized spin-dependent interaction strength defined as $r=(a_2-a_0)/(a_0+2a_2)$, where a_0 and a_2 are the s-wave scattering lengths in the symmetric channels with total spin of the colliding atoms $F=0$ and $F=2$, respectively. Note that $r<0$ and $r>0$ correspond, respectively, to ferromagnetic and polar spinor BECs. In the relevant cases of ^{87}Rb and ^{23}Na atoms with $F=1$, this parameter takes values $r=-4.66\times 10^{-3}$ [28] and $r=+3.14\times 10^{-2}$ [29], respectively, i.e., in either case, it is a small parameter in Eqs. (1) and (2).

We now seek uniform stationary solutions of the GP Eqs. (1) and (2) (with $V=0$) in the form

$$\psi_1 = A\exp(-i\mu_{+1}t)\exp(i\theta_{+1}),$$

$$\psi_0 = B\exp(-i\mu_0 t)\exp(i\theta_0),$$

$$\psi_{-1} = C\exp(-i\mu_{-1}t)\exp(i\theta_{-1}),$$

where A, B, C, and θ_j (with $j\in\{-1,0,+1\}$) represent, respectively, the amplitudes and phases of the hyperfine components, and μ_j are their chemical potentials. In our analysis below we will assume that $A\neq 0$, $B\neq 0$, and $C\neq 0$, as that will provide us with genuinely spinor (i.e., three-component) states; otherwise the system is reduced to a lower number of components. In fact, the analysis for the one-component case has been carried out in Ref. [19] while, in the two-component case, considerations analogous to the ones that we will present below have been put forth in Ref. [27]. Under the above genuinely three-component assumption, we substitute the stationary solutions into GP Eqs. (1) and (2) and obtain the following set of equations:

$$\mu_{+1} = n_{\mathrm{tot}} + r(A^2+B^2-C^2) + pr\frac{B^2C}{A},$$

$$\mu_0 = n_{\mathrm{tot}} + r(A^2+C^2) + 2prAC,$$

$$\mu_{-1} = n_{\mathrm{tot}} + r(C^2+B^2-A^2) + pr\frac{B^2A}{C},$$

where $n_{\mathrm{tot}}=A^2+B^2+C^2$.

In the above expressions phase matching conditions were used, as is usual when one has parametric interactions: these read $2\mu_0=\mu_{+1}+\mu_{-1}$ for the chemical potentials, and $\Delta\theta=2\theta_0-(\theta_{+1}+\theta_{-1})=0$ or π for the relative phase between the hyperfine components [18,30]. The factor $p\equiv\pm 1$ on the last term of each of the above equations results from considering $\Delta\theta=0$ or π, respectively. In the case where the three chemical potentials μ_j are different, it can be found that it is not possible to satisfy the above assumption that each of the amplitudes A, B, and C should be nonzero. Hence, we will hereafter focus on the case of $\mu_{+1}=\mu_0=\mu_{-1}\equiv\mu$. In the latter case, it is straightforward to algebraically manipulate the equations and find that there exist only two classes of possible stationary solutions with a free parameter (for a given μ). These solutions are as follows:

$$A = -pC, \quad B = \pm\sqrt{\mu - 2C^2}, \quad \mu > 2C^2, \tag{4}$$

$$A = -pC \pm \sqrt{\frac{\mu}{1+r}}, \quad B = \pm\sqrt{2pAC}, \quad \mu > 1 + r, \tag{5}$$

and are simply the "anti-phase-matched" and "phase-matched" type solutions of Ref. [31], respectively. Note that in addition to these solutions, there exists another one with no free parameters (i.e., all amplitudes are directly dependent on μ) which is a particular case of Eq. (5), namely,

$$A = pC, \quad B = \pm\sqrt{2C^2}, \quad \mu = 4(1+r)C^2. \tag{6}$$

Let us now consider GP Eqs. (1) and (2); looking for stationary solutions in that frame, the GP equations become

$$-is\partial_x\psi_{\pm1} = -\frac{1}{2}\partial_x^2\psi_{\pm1} + n_{\text{tot}}\psi_{\pm1} + r(|\psi_{\pm1}|^2 + |\psi_0|^2 - |\psi_{\mp1}|^2)\psi_{\pm1} + r\psi_0^2\psi_{\mp1}^* - \mu\psi_{\pm1}, \tag{7}$$

$$-is\partial_x\psi_0 = -\frac{1}{2}\partial_x^2\psi_0 + n_{\text{tot}}\psi_0 + r(|\psi_{-1}|^2 + |\psi_{+1}|^2)\psi_0 + 2r\psi_{-1}\psi_0^*\psi_{+1} - \mu\psi_0, \tag{8}$$

where we have slightly abused the notation by replacing the traveling-wave variable $\xi = x - st$ with x for simplicity. We now decompose the amplitudes R_j and phases ϕ_j of the order parameters according to $\psi_j = R_j\exp(i\phi_j)$, and impose the phase matching condition $\phi_1 + \phi_{-1} = 2\phi_0$ to obtain the following equations:

$$\partial_x\phi_1 = s\left[1 - \left(\frac{A}{R_1}\right)^2\right], \tag{9}$$

$$\partial_x^2 R_1 = -s^2\left(R_1 - \frac{A^4}{R_1^2}\right) + 2n_{\text{tot}}R_1 + 2r(R_1^2 + R_0^2 - R_{-1}^2)R_1 + 2prR_0^2R_{-1} - 2\mu R_1, \tag{10}$$

$$\partial_x\phi_0 = s\left[1 - \left(\frac{B}{R_0}\right)^2\right], \tag{11}$$

$$\partial_x^2 R_0 = -s^2\left(R_0 - \frac{B^4}{R_0^2}\right) + 2n_{\text{tot}}R_0 + 2r(R_1^2 + R_{-1}^2)R_0 + 4prR_0R_1R_{-1} - 2\mu R_0, \tag{12}$$

$$\partial_x\phi_{-1} = s\left[1 - \left(\frac{C}{R_{-1}}\right)^2\right], \tag{13}$$

$$\partial_x^2 R_{-1} = -s^2\left(R_{-1} - \frac{C^4}{R_{-1}^2}\right) + 2n_{\text{tot}}R_{-1} + 2r(R_{-1}^2 + R_0^2 - R_1^2)R_{-1} + 2prR_0^2R_1 - 2\mu R_{-1}. \tag{14}$$

Notice that in these equations, the asymptotic states A, B, and C arise naturally due to the integration of the equations for the phases.

In order to seek instabilities of the steady-state flow at different fluid speeds, we now linearize around the asymptotic states, according to $R_1 = A + \epsilon r_1(x)$, $R_0 = B + \epsilon r_0(x)$, and $R_{-1} = C + \epsilon r_{-1}(x)$ (where ϵ is a formal small parameter). Substituting the above expressions into Eqs. (9)–(15), we obtain a system of three second-order ordinary differential equations; the latter can be readily expressed as a system of six first-order equations of the following form:

$$\frac{d}{dx}\begin{pmatrix} r_1 \\ r_1' \\ r_2 \\ r_2' \\ r_3 \\ r_3' \end{pmatrix} = M\begin{pmatrix} r_1 \\ r_1' \\ r_2 \\ r_2' \\ r_3 \\ r_3' \end{pmatrix},$$

where $r_j' \equiv dr_j/dx$ and

$$M \equiv \{m_{ij}\} = \begin{pmatrix} 0 & 1 & 0 & 0 & 0 & 0 \\ m_{21} & 0 & m_{23} & 0 & m_{25} & 0 \\ 0 & 0 & 0 & 1 & 0 & 0 \\ m_{41} & 0 & m_{43} & 0 & m_{45} & 0 \\ 0 & 0 & 0 & 0 & 0 & 1 \\ m_{61} & 0 & m_{63} & 0 & m_{65} & 0 \end{pmatrix},$$

and the nonzero matrix elements of M are given by the following expressions:

$$m_{21} = -4s^2 + 2(3A^2 + B^2 + C^2) + 2r(3A^2 + B^2 - C^2) - 2\mu,$$

$$m_{23} = m_{41} = 4AB(1+r) + 4prBC,$$

$$m_{25} = m_{61} = 4AC(1-r) + 2prB^2,$$

$$m_{43} = -4s^2 + 2(3B^2 + A^2 + C^2) + 2r(A^2 + C^2) + 4prAC - 2\mu,$$

$$m_{45} = m_{63} = 4BC(1+r) + 4prAB,$$

$$m_{65} = -4s^2 + 2(3C^2 + B^2 + A^2) + 2r(3C^2 + B^2 - A^2) - 2\mu.$$

Notice that, in order to derive the above system of ordinary differential equations, we have partially simplified the problem, assuming no perturbations in the phases. In such a more general case, however, the full first-order ordinary differential equation (ODE) system incorporating phase perturbations is in fact twelve-dimensional and is not analytically tractable. We have found (not treated explicitly here) that this system can be analyzed only in some special cases, such as $B=0$, yielding the same results for the critical defect speeds, as will be presented below (see also the discussion of Sec. II B in Ref. [17]).

We now follow the approach used for the one-component GP equation in Ref. [19] (subsequently generalized in the two-component case in Ref. [27]) to determine the critical speeds of the defect. In particular, the critical speeds can readily be found upon computing the eigenvalues of the matrix M and setting them equal to zero. The violation of this threshold condition is tantamount to the emergence of a number of oscillatory modes that enforce too many constraints and prevent the existence of localized solutions for a generic obstacle potential, as is explained in detail in Ref. [19]. It is straightforward to examine this condition both in the case of $p=1$ and of $p=-1$. We will demonstrate below the case of $p=1$ for definiteness. In this case, by considering the stationary state of the form of Eq. (4), we obtain two different speeds of sound, namely,

$$c_1 = \sqrt{r}c_2, \quad c_2 = \sqrt{\mu}. \tag{15}$$

It is clear that the first critical velocity is characteristic for the spinor $F=1$ condensate under consideration (as it depends on the normalized spin-dependent interaction strength r) while the second one is the standard speed of sound appearing in the one-component GP equation [19]. Note that these speeds of sound were already implicit in the seminal work of Ref. [32] (see, e.g., Eqs. (8)–(11) therein and the accompanying discussion, as well as the more recent discussion of Sec. II B in [17]). It is worthwhile to point out that as $r>0$ for *antiferromagnetic* bosonic spin-1 atoms (e.g., ^{23}Na) while it is $r<0$ for *ferromagnetic* ones (e.g., ^{87}Rb), then the first speed of sound is relevant (i.e., will only exist) in the case of, e.g., the polar ^{23}Na spinor condensate. On the other hand, by selecting the stationary states of the form of Eq. (5), then again we find two critical speeds, which are now given by

$$c_1 = \sqrt{\frac{-r}{1+r}}c_2, \quad c_2 = \sqrt{\mu}. \tag{16}$$

In this case, it is clear that the first critical speed will exist only in the ferromagnetic spinor BECs (such as ^{87}Rb) but not in antiferromagnetic ones (such as ^{23}Na); nevertheless, it should be noted that since the normalized spin-dependent interaction strength is small in both cases of ^{87}Rb and ^{23}Na condensates [$r=O(10^{-2})$ as discussed above], the lower critical speeds are approximately the same.

We now test these analytical predictions by dragging a localized defect (e.g., a blue-detuned laser beam) through the condensate at different speeds characterizing the three regimes, namely, (a) $0<s<c_1<c_2$, (b) $c_1<s<c_2$, and (c) $c_1<c_2<s$.

III. RESULTS OF NUMERICAL STUDIES

A. One-dimensional setting

Our more detailed results concern the 1D setting, where we explore the full two-parameter space of speeds s and defect strengths V_0, for $a=2$ in the case of the antiferromagnetic ^{23}Na spinor BEC, characterized by the spin-dependent interaction strength $r=0.0314$. Figure 1 illustrates the threshold above which coherent localized excitations are emitted from the defect as it propagates through the condensate. A typical example of the evolution process for (a) $0<s=0.025<c_1<c_2$, (b) $c_1<s=0.325<c_2$, and (c) $c_1<c_2<s=0.335$ is shown in Fig. 2. Several comments are in order here:

(i) As expected from the analytical predictions, when the defect speed is below both critical values $c_1=\sqrt{\mu r}$ and $c_2=\sqrt{\mu}$, the defect moves through the atomic cloud without emission of any nonlinear excitation. An oscillatory structure is radiated at the initial time (similarly to what has been observed earlier, e.g., in Ref. [27]) both at the front, as well as at the rear of the defect, moving with the speed of sound; however, no further such radiation is observed.

(ii) Remarkably, for speeds intermediate between c_1 and c_2, we do *not* observe any modification in the dynamics. This means that the first critical speed c_1 does not appear to be

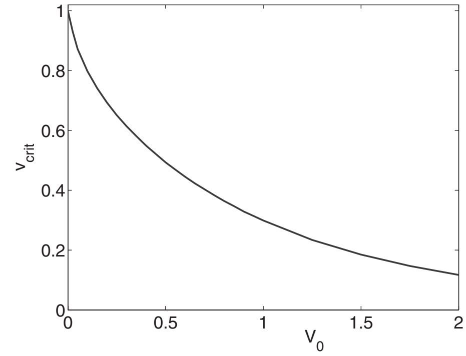

FIG. 1. Dependence of the critical velocity on the defect strength V_0. The result shown corresponds to the stationary solution of Eq. (4) with $A=-0.5=-C$ and $B=\sqrt{1/2}(\mu=1)$. It was confirmed that, e.g., for the solutions of Eq. (5), the analytical and numerical results were indistinguishable up to three decimal places.

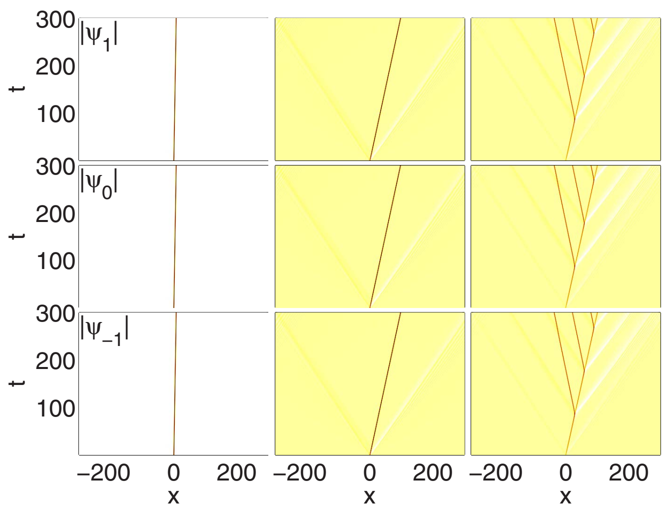

FIG. 2. (Color online) Time evolution of the three hyperfine components (top, middle, and bottom rows, respectively) for different defect velocities: $s=0.025<c_1$ (left column), $c_1<s=0.325\lesssim c_2$ (middle column), and $s=0.335>c_2$ (right column); here, $c_1=0.058$ and $c_2=0.329$ are the two critical velocities while the defect strength is taken to be $V_0=0.9$. The initial condition corresponds to the stationary state with wave-function amplitudes given in Eq. (4). While the results in the left and middle columns show a steady flow (apart from an oscillatory structure that is detached at $t=0$), the evolution shown in the panels of the right column is characterized by the emission of dark solitons, even from the early stages of the process. Notice that the analytically predicted first (lower) critical velocity would fall between the velocities of the results depicted in the left and middle columns but no significant change is observed in the dynamics between these two cases.

activated by the system. This finding is even more surprising in light of the fact that, for $r<0$, this critical speed has been recognized to be directly connected to the quasimomentum (wave number) associated with the modulational instability of the ferromagnetic spinor condensate [30] (see also the relevant discussion in Ref. [17]). Nevertheless, in all of our simulations, both in 1D and in higher dimensions, we have definitively confirmed the apparent physical irrelevance of this first critical speed (which is the lower nontrivial critical speed in the spinor BEC case). It should be noted here that this same feature has been confirmed for cases where the spin-dependent interaction strength r was artificially increased to considerably larger values (by an order of magnitude in comparison with its physically relevant value of $r=3.14\times10^{-2}$ for ^{23}Na). From a physical perspective, a potential explanation of this feature can stem from the fact that this speed is associated with spin excitations [32] rather than density excitations (from the latter one would normally anticipate the emergence/emission of nonlinear excitations, as is the case in the two-component system studied in Ref. [27]).

(iii) When the defect speed is larger than both critical ones, there is a clear emission of dark (in fact, gray) solitons, which travel in a direction opposite to that defect, with velocities less than the speed of sound. Similarly to one-component [19–22] and two-component [27] settings, the solitons temporarily "alleviate" the supercritical nature of the flow but eventually they are separated enough from the defect that another such excitation emerges. For this reason, the emission seems to be regularly spaced as shown in the right panels of Fig. 2.

(iv) As the strength of the defect $V_0\to0$, the critical speed c_2 observed from the numerical simulations tends asymptotically to the one theoretically predicted from the analysis above, i.e., $\sqrt{\mu}=1$ in this case (this feature has been confirmed for different values of μ, such as $\mu=2$ and $\mu=4$). However, similarly to what was observed in Refs. [19,27], as the strength of the defect increases, the value of the critical speed accordingly decreases (since nucleation of dark solitons is easier for the lower density BEC).

(v) Finally, we note that in all our simulations (even in higher dimensions, see below) the three spinor components were locked to each other through $|\psi_1|^2/A^2\approx|\psi_0|^2/B^2\approx|\psi_{-1}|^2/C^2$. This tight restriction is presumably related to the fact that we only observed one critical nucleation speed in our simulations: as all the components are tightly locked to each other, they behave like a single component and thus only one critical speed is observed.

B. Two-dimensional setting

In the 2D case, motivated by the recent work of Ref. [23] in the single-component case, we consider a defect which is localized along the x axis (with a width a^{-1}) but elongated along the y axis (with a width $w_y>a^{-1}$), namely:

$$V=\frac{V_0}{4}\exp[-a(x-st)^2]\left[\tanh\left(y+\frac{w_y}{2}\right)+1\right]\times\left[\tanh\left(-y+\frac{w_y}{2}\right)+1\right].$$

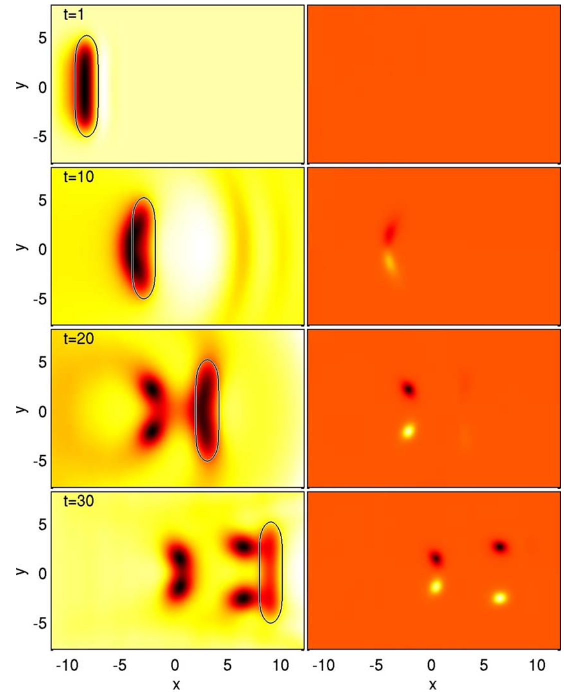

FIG. 3. (Color online) Vortex and antivortex pairs nucleated by a moving defect in the 2D spinor condensate. The left column shows the density of the spinor condensate's component ψ_0 at different times (indicated in the panels). The location and extent of the moving defect is depicted by the oval line corresponding to an isocontour of its strength at 10% of its maximum. The right column shows the corresponding vorticity (defined in the text), clearly illustrating the presence of vortex and antivortex pairs. The case depicted here corresponds to $w_y=8$, $a=2$, and $V_0=0.9$ while the defect speed is taken to be $s=0.6>c_2$.

Once again, we find that (i) no emission of nonlinear excitations is present for $s<c_2$ and that (ii) the emission of nonlinear excitations, which now have the form of vortex-antivortex pairs, arises for speeds larger than the critical speed c_2. Figure 3 illustrates the case of $s=0.6>c_2$ for the defect strength $V_0=0.9$ while the defect width along the y direction is $w_y=8$. In addition to showing the density, the figure shows the vorticity defined as $\omega=\nabla\times v_f$, where the fluid velocity v_f is given by

$$v_f=\frac{\psi^\star\nabla\psi-\psi\nabla\psi^\star}{i|\psi|^2}, \tag{17}$$

for a given hyperfine component ψ. In the contour plots of the vorticity ω, the emergence of vortex-antivortex pairs is immediately evident in the supercritical case shown. In fact, in order to provide a more clear sense of the temporal dynamics and the nucleation of the coherent structure pairs, we show in the left panel of Fig. 4 the spatiotemporal evolution of the isocontours of vorticity for the same numerical simulation as in Fig. 3. The vorticity renders transparent the emergence of the different vortex pairs at different moments in time (and accordingly different locations in x, as the defect travels).

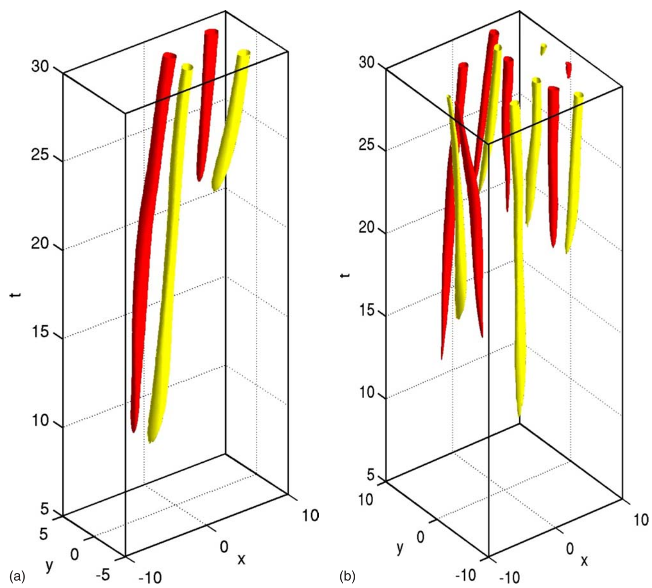

FIG. 4. (Color online) Evolution of the maximum (dark/red) and minimum (light/yellow) of the vorticity isocontours in (x,y,t). One can clearly discern the emergence of vortex (in dark/red) and antivortex (in light/yellow) pairs, as the defect moves along the x direction. The left and right panels correspond, respectively, to the cases depicted in Fig. 3 (w_y=8) and Fig. 5 (w_y=20).

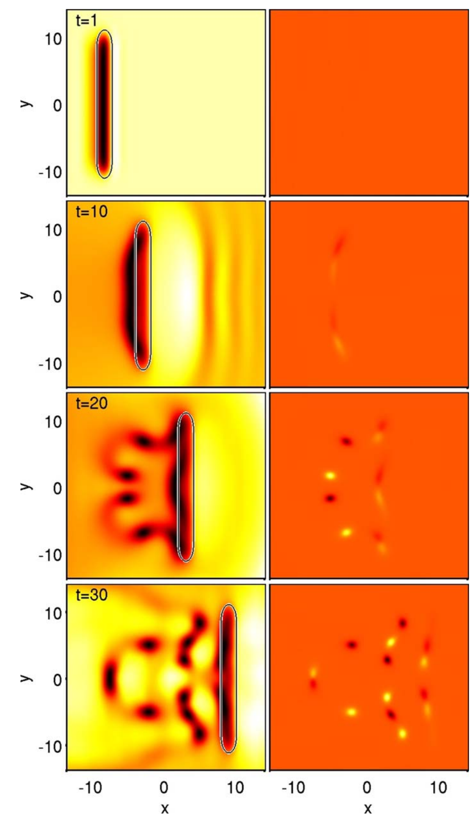

FIG. 5. (Color online) Same as Fig. 3 but for a wider defect with w_y=20. One can clearly observe the formation of numerous vortex-antivortex pairs in the wake of the defect.

Finally, in Fig. 5, we also show a case example of a considerably wider defect, with a width w_y=20. It can be seen that in this setting, the region of low density caused by the defect is far wider, in turn leading to a breakup into a large number of vortex pairs that can be identified not only by the density minima but also even more clearly (including their topological charge) by the vorticity panels. In the right panel of Fig. 4 we depict the corresponding spatiotemporal evolution of the vorticity. We note that, as it was the case in the 1D setting, all our simulations suggest that the three spinor components remain essentially locked satisfying the relation $|\psi_1|^2/A^2 \approx |\psi_0|^2/B^2 \approx |\psi_{-1}|^2/C^2$. For this reason, we only depict the dynamics of the ψ_0 component in all of our results.

C. Three-dimensional setting

Finally, we also performed 3D simulations, using a three-dimensional generalization of the potential, elongated along the z direction, namely,

$$V = \frac{V_0}{16}\exp[-a(x-st)^2]\left[\tanh\left(y+\frac{w_y}{2}\right)+1\right] \times\left[\tanh\left(-y+\frac{w_y}{2}\right)+1\right]\left[\tanh\left(z+\frac{w_z}{2}\right)+1\right] \times\left[\tanh\left(-z+\frac{w_z}{2}\right)+1\right],$$

with a=2, w_y=8, w_z=4, and V_0=0.9. In Fig. 6 we depict the results for s=0.8 (i.e., above the second critical speed). Panels (a)–(e) depict the isodensity contours for $|\psi_0|^2$ at different times while panel (f) depicts a superposition of the isocontours for the norm of the vorticity field. As it can be seen from the figure, a vortex ring is formed in the 3D spinor condensate, as a result of the supercritical nature of the chosen speed $s=0.8>c_2$. The isodensity contours of $|\psi_0|^2$ clearly show a depletion of atoms around the vortex ring that is nucleated in the wake of the defect-induced region of density minima. It is worth stressing again that the dynamics of the different components seems to be locked such that $|\psi_1|^2/A^2 \approx |\psi_0|^2/B^2 \approx |\psi_{-1}|^2/C^2$ and, therefore, we only depict results for ψ_0 in the 3D case as well.

We also performed simulations for larger defect speeds giving rise to a rich and complex scenario of multiple vortex rings nucleations, collisions, collapses, and splitting. A typical case is shown in Fig. 7 that corresponds to the same parameters as in Fig. 6 but for a larger defect speed (s=1). The main characteristics of the evolution can be summarized as follows: a first vortex ring is nucleated in the wake of the defect at about t=12; around t=17 a second vortex ring is nucleated while the first vortex ring starts to shrink until it eventually disappears around t=23; shortly after this, the second ring deforms and splits into two separate vortex rings around t=30.

IV. CONCLUSIONS AND FUTURE CHALLENGES

We have studied the motion of a localized defect through a spinor F=1 condensate. Despite the three-component nature of the system, our systematic analysis of the small-amplitude excitation problem revealed that the nature of the

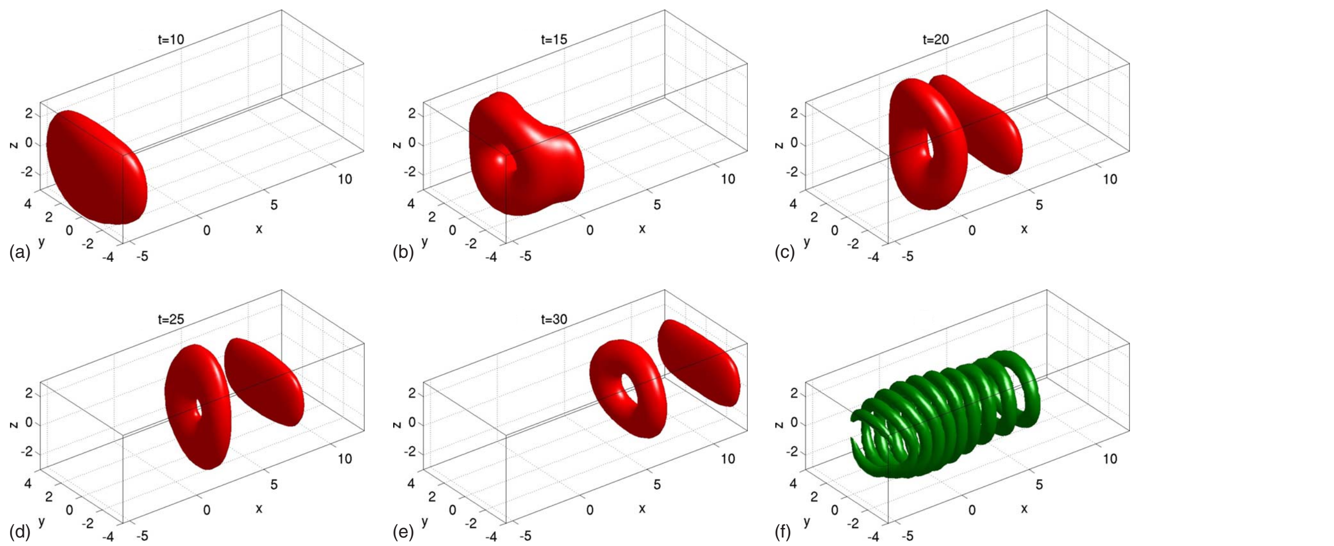

FIG. 6. (Color online) Vortex ring formation in the supercritical 3D setting. Panels (a)–(e) depict isodensity contours corresponding to $|\psi_0|^2=0.3$ at the indicated times. Note that the extent of the moving defect is clearly visible in these panels (it corresponds to the rightmost flat oval shape that is created by the atomic density depletion due to its presence). Panel (f) shows typical isocontours of the norm of the vorticity of ψ_0 at times $t=12,14,\ldots,30$ (left to right). In this case we use a defect with $w_y=8$, $w_z=4$, $a=2$, and speed $s=0.8>c_2$.

nonlinearity is such that there appear not three but merely two critical speeds in the system; these were identified analytically for the families of stationary uniform states of the system. Our numerical simulations tested the dynamics for different values of defect speeds in comparison to the two critical speeds. Surprisingly, it was found that the lower one among the two critical speeds is *not* activated and no emission of nonlinear wave excitations emerges when this threshold is crossed. On the other hand, when the defect speed exceeds the second critical one, then emission of coherent structures arises independently of dimension; the resulting wave forms are dark solitons in the one-dimensional setting, vortex-antivortex pairs in two dimensions, and spinor vortex rings in the fully three-dimensional case.

While the present study showcases an experimentally accessible mechanism for producing nonlinear excitations in spinor BECs, a number of interesting questions are still outlying. In particular, perhaps the most relevant question from a mathematical point of view involves acquiring a rigorous explanation of why the first critical speed does not seem to be explored by the system, contrary to what is found in the two-component case analyzed in Ref. [27]. Another direction of potential interest could be to explore in this multicomponent system what would happen if the speed of the defect becomes considerably larger than the critical speed, in which case, and in the one-component setting, a convective stabilization of oblique dark solitons has been reported [33]. Also interesting would be to study the formation of shock waves [34] in the spinor systems. Work along these directions is currently in progress and will be reported in future publications.

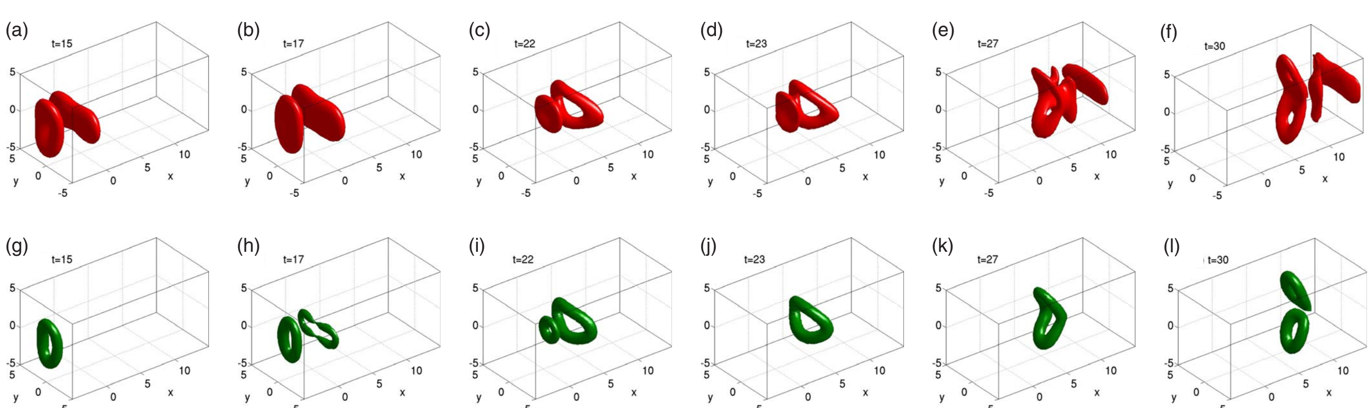

FIG. 7. (Color online) Similar to Fig. 6 but for a slightly larger defect speed $s=1>c_2$. The top row of panels depicts the isodensity contours of ψ_0 while the bottom row depicts the respective vorticity isocontours. Note the successive nucleation of two vortex rings. The first one shrinks and collapses into itself between $t=22$ and $t=23$ while the second ring deforms and eventually splits into two separate vortex rings between $t=29$ and $t=30$.

ACKNOWLEDGMENTS

The authors (P.G.K, T.J.A., and Y.S.K.) acknowledge useful discussions with Elena Ostrovskaya. The work in Australia was supported by the Australian Research Council through the Australian Center for Quantum-Atom Optics (ACQAO) of the Australian Research Council. P.G.K. and R.C.G. gratefully acknowledge support from NSF grant no. DMS-0806762, and P.G.K. also acknowledges support from the NSF-CAREER program and the Alexander von Humboldt Foundation. The work of D.J.F. was partially supported by the Special Research Account of the University of Athens. The work of A.S.R. was partially supported by FCT through grant no. POCTI/FIS/56237/2004.

[1] C. J. Pethick and H. Smith, *Bose-Einstein Condensation in Dilute Gases* (Cambridge University Press, Cambridge, 2002).
[2] L. P. Pitaevskii and S. Stringari, *Bose-Einstein Condensation* (Oxford University Press, Oxford, 2003).
[3] *Emergent Nonlinear Phenomena in Bose-Einstein Condensates. Theory and Experiment*, edited by P. G. Kevrekidis, D. J. Frantzeskakis, and R. Carretero-González (Springer-Verlag, Berlin, 2008).
[4] D. M. Stamper-Kurn, M. R. Andrews, A. P. Chikkatur, S. Inouye, H.-J. Miesner, J. Stenger, and W. Ketterle, Phys. Rev. Lett. **80**, 2027 (1998).
[5] M.-S. Chang, C. D. Hamley, M. D. Barrett, J. A. Sauer, K. M. Fortier, W. Zhang, L. You, and M. S. Chapman, Phys. Rev. Lett. **92**, 140403 (2004).
[6] D. M. Stamper-Kurn and W. Ketterle, in *Coherent Atomic Matter Waves*, edited by R. Kaiser, C. Westbrook, and F. David, Vol. 72 of Les Houches Summer School, p. 137, e-print arXiv:cond-mat/0005001.
[7] J. Stenger, S. Inouye, D. M. Stamper-Kurn, H.-J. Miesner, A. P. Chikkatur, and W. Ketterle, Nature (London) **396**, 345 (1998).
[8] A. E. Leanhardt, Y. Shin, D. Kielpinski, D. E. Pritchard, and W. Ketterle, Phys. Rev. Lett. **90**, 140403 (2003).
[9] H. Pu, C. K. Law, S. Raghavan, J. H. Eberly, and N. P. Bigelow, Phys. Rev. A **60**, 1463 (1999).
[10] S. Yi, Ö. E. Müstecaplioglu, and L. You, Phys. Rev. A **68**, 013613 (2003).
[11] Ö. E. Müstecaplioglu, M. Zhang, S. Yi, L. You, and C. P. Sun, Phys. Rev. A **68**, 063616 (2003).
[12] J. Ieda, T. Miyakawa, and M. Wadati, Phys. Rev. Lett. **93**, 194102 (2004); J. Phys. Soc. Jpn. **73**, 2996 (2004).
[13] L. Li, Z. Li, B. A. Malomed, D. Mihalache, and W. M. Liu, Phys. Rev. A **72**, 033611 (2005).
[14] W. Zhang, Ö. E. Müstecaplioglu, and L. You, Phys. Rev. A **75**, 043601 (2007).
[15] M. Uchiyama, J. Ieda, and M. Wadati, J. Phys. Soc. Jpn. **75**, 064002 (2006).
[16] B. J. Dabrowska-Wüster, E. A. Ostrovskaya, T. J. Alexander, and Yu. S. Kivshar, Phys. Rev. A **75**, 023617 (2007).
[17] H. E. Nistazakis, D. J. Frantzeskakis, P. G. Kevrekidis, B. A. Malomed, and R. Carretero-González, Phys. Rev. A **77**, 033612 (2008).
[18] H. E. Nistazakis, D. J. Frantzeskakis, P. G. Kevrekidis, B. A. Malomed, R. Carretero-González, and A. R. Bishop, Phys. Rev. A **76**, 063603 (2007).
[19] V. Hakim, Phys. Rev. E **55**, 2835 (1997).
[20] A. Radouani, Phys. Rev. A **70**, 013602 (2004).
[21] G. Theocharis, P. G. Kevrekidis, H. E. Nistazakis, D. J. Frantzeskakis, and A. R. Bishop, Phys. Lett. A **337**, 441 (2005).
[22] R. Carretero-González, P. G. Kevrekidis, D. J. Frantzeskakis, B. A. Malomed, S. Nandi, and A. R. Bishop, Math. Comput. Simul. **74**, 361 (2007).
[23] P. Engels and C. Atherton, Phys. Rev. Lett. **99**, 160405 (2007).
[24] T. Frisch, Y. Pomeau, and S. Rica, Phys. Rev. Lett. **69**, 1644 (1992); B. Jackson, J. F. McCann, and C. S. Adams, *ibid.* **80**, 3903 (1998); T. Winiecki, J. F. McCann, and C. S. Adams, *ibid.* **82**, 5186 (1999).
[25] C. Raman, M. Köhl, R. Onofrio, D. S. Durfee, C. E. Kuklewicz, Z. Hadzibabic, and W. Ketterle, Phys. Rev. Lett. **83**, 2502 (1999); R. Onofrio, C. Raman, J. M. Vogels, J. R. Abo-Shaeer, A. P. Chikkatur, and W. Ketterle, *ibid.* **85**, 2228 (2000).
[26] N. Pavloff, Phys. Rev. A **66**, 013610 (2002); M. Albert, T. Paul, N. Pavloff, and P. Leboeuf, Phys. Rev. Lett. **100**, 250405 (2008).
[27] H. Susanto, P. G. Kevrekidis, R. Carretero-González, B. A. Malomed, D. J. Frantzeskakis, and A. R. Bishop, Phys. Rev. A **75**, 055601 (2007).
[28] E. G. M. van Kempen, S. J. J. M. F. Kokkelmans, D. J. Heinzen, and B. J. Verhaar, Phys. Rev. Lett. **88**, 093201 (2002).
[29] N. N. Klausen, J. L. Bohn, and C. H. Greene, Phys. Rev. A **64**, 053602 (2001).
[30] N. P. Robins, W. Zhang, E. A. Ostrovskaya, and Yu. S. Kivshar, Phys. Rev. A **64**, 021601(R) (2001).
[31] M. Matuszewski, T. J. Alexander, and Yu. S. Kivshar, Phys. Rev. A **78**, 023632 (2008).
[32] T.-L. Ho, Phys. Rev. Lett. **81**, 742 (1998).
[33] G. A. El, A. Gammal, and A. M. Kamchatnov, Phys. Rev. Lett. **97**, 180405 (2006); A. M. Kamchatnov and L. P. Pitaevskii, *ibid.* **100**, 160402 (2008).
[34] Z. Dutton, M. Budde, C. Slowe, and L. V. Hau, Science **293**, 663 (2001); T. P. Simula, P. Engels, I. Coddington, V. Schweikhard, E. A. Cornell, and R. J. Ballagh, Phys. Rev. Lett. **94**, 080404 (2005); M. A. Hoefer, M. J. Ablowitz, I. Coddington, E. A. Cornell, P. Engels, and V. Schweikhard, Phys. Rev. A **74**, 023623 (2006).